PHYSICAL SCIENCE OF MATERIALS

UDC 534-16 PACS: 62.25.−g
EDN: OFPCRC

Study of acoustic properties of van der Waals heterostructures containing the WSe_2 monolayer using the hypersonic microscopy

© N. Yu. Frolov*, A. Y. Klokov, A. I. Sharkov, S. N. Nikolaev, M. A. Chernopitsky, S.I. Chentsov, M. V. Pugachev, A. V. Shupletsov, V. S. Krivobok, A. Y. Kuntsevich

Lebedev Physical Institute of the Russian Academy of Sciences, Moscow, 119991 Russia
**E-mail: frolil199999@gmail.com*

Received 18.10.2024; revised 09.12.2024; accepted 14.04.2025
Scientific specialty code: 1.3.7

Elastic properties of the layered heterostructure of Al/hBN/WSe_2(monolayer)/hBN/Al_2O_3 were studied using a picosecond ultrasonic technique. Time dependences of the change in the phase of the reflection coefficient of the sample caused by propagation of the elastic pulse excited by a femtosecond laser were measured during the experiment. A map built to describe the spatial distribution of the modulus of the response Fourier spectrum components for different frequencies allowed to localize the region of the heterostructure containing the WSe_2 monolayer. By means of a mathematical model of the multilayer structure response, the elastic parameters of heterostructure Al/hBN/WSe_2(monolayer)/hBN/Al_2O_3 were estimated, in particular rigidities of layer interfaces.

Keywords: picoacoustics; laser hypersound; mechanical properties; van der Waals heterostructures; monolayer.

DOI: 10.51368/1996-0948-2025-90-96

Introduction

In recent years, the use of van der Waals (VdW) materials in micro- and nanoelectronics has been advancing incrementally. This trend is primarily caused by the wide range of unique properties exhibited by such materials. Forming heterostructures based on such properties enables the significant setting up of characteristics of final optical and electronic devices as well as their compact arrangement and higher efficiency [2, 3].

For example, transition metal dichalcogenides (TMDs) that are an advanced platform for atomically thin flexible optoelectronics [4, 5] have become widely popular. Monochalcogenide compounds are also of great interest for use in visible and near IR photodetectors due to their narrow-forbidden band [6]. Graphene is demonstrating its potential as an element of atomically thin tactile sensors [7], acoustic coatings [8], and elements of micro- [9] and nanoelectromechanical [10] systems.

It should be noted that assembling van der Waals heterostructures requires high precision [11], since the performance of such heterostructures is strongly dependent on both the lateral homogeneity of layers themselves and quality of their interfaces influencing the mechanical and acoustic properties of the

structure. They, in turn, may have significant influence on the transport of charge carriers and phonons, for which reason such studies are of high priority.

Today, the most effective approach for studying the mechanical and acoustic properties of van der Waals heterostructures is the picosecond acoustics method, where an optically excited short elastic pulse is used as a tool for diagnosing materials. This elastic pulse propagates deeply into the sample and is partially reflected at the interfaces. The coefficient of elastic pulse reflection from the layers interface is also dependent on the quality of contact between the VdW layers [12, 13].

In this paper we focused on studying the acoustic properties of heterostructure Al/hBN/WSe_2(monolayer)/hBN/hBN/Al_2O_3 and its interfaces, as well as the influence of the WSe_2 monolayer on the elastic pulse spectrum characteristics within the heterostructure.

Experiment description

This paper provides the results of studying the heterostructure containing the WSe_2 monolayer encapsulated between thin layers (~12 nm) of hBN (Fig. 1*a*). hBN layers were produced by peeling off with a Scotch tape on oxidized Si. While the WSe_2 monolayer was produced by the laminating method using gold, which is described in [14]. Then, the heterostructure was assembled on the Al_2O_3 substrate with (001) orientation by dry hot transfer [15] in ambient conditions. A thin Al film (~30 nm thick) sprayed on by electron beam evaporation acted as a generator of elastic pulses in the structure upon absorption of laser radiation. The layers were characterized by means of atomic force microscopy during assembly of the heterostructure. The WSe_2 monolayer was identified using Raman scattering spectroscopy and photoluminescence measurements (Fig. 1*b*) [16].

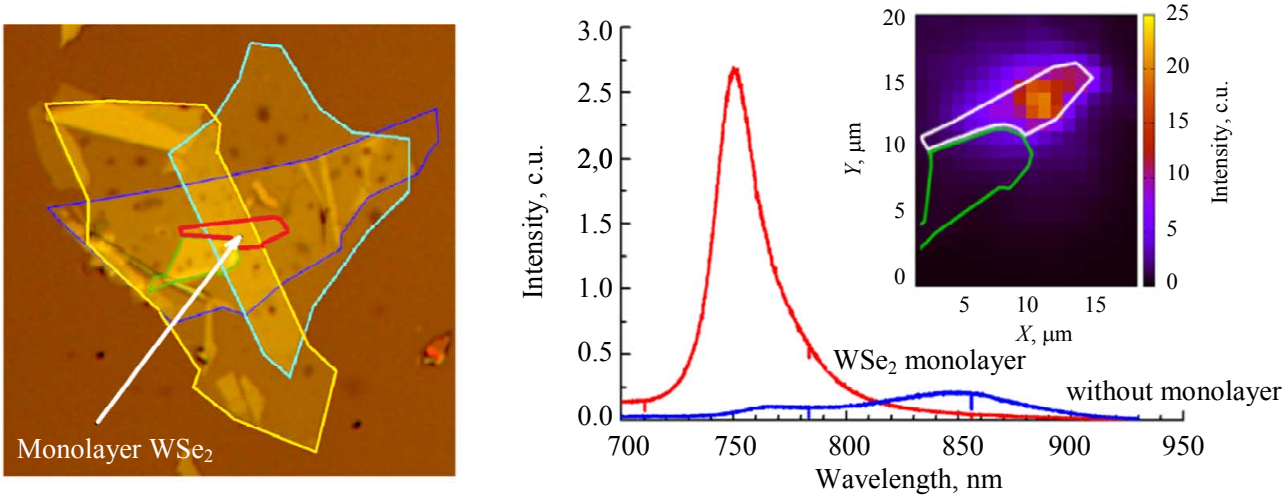

a) *b*)

Fig. 1. a) – photo of the structure: the region where the WSe_2 monolayer was located is red, blue, hBN layers are yellow and light blue, WSe_2 layer is green, multilayer $Wse2_2$ is green; b) – photoluminescence spectra of mono- and multilayer WSe_2 at 300 K; the inset shows the spatial map of photoluminescence in the wavelength range of 738–760 nm after excitation at the wavelength of 472 nm

Pulses of coherent phonons in the heterostructure were optically generated and recorded using a two-colour pump-probe setup (Fig. 2), which allowed measuring changes in the complex reflection coefficient with temporal and spatial resolution. The source of laser radiation was a femtosecond Ti:Sa laser generating pulses of linearly polarized radiation at the wavelength λ = 800 nm with a duration τ_{pulse} = 160 fs and

repetition frequency of f = 76 MHz. The second harmonic laser pulse of the source, when absorbed by aluminum, generated a picosecond elastic pulse that propagated perpendicularly to the surface deeply into the sample and was partially reflected from the heterostructure interfaces. Propagation of the elastic pulse, in turn, caused changes in the sample's reflection coefficient recorded with the second light pulse at the wavelength of the source, which was focused at the same point as the excitation pulse.

The experiment measured the time dynamics of the reflection coefficient phase in different areas of the structure by means of a delay line that allowed changing the time delay of the probing pulse relative to the excitation pulse. Due to use of the Sagnac interferometer the sensitivity of the setup to minor phase changes was increased significantly [17].

The resulting responses were a combination of a high-oscillating part associated with propagation of the elastic pulse in the structure and a slow thermal contribution. After the slow component was substracted, the Fourier spectral analysis of the obtained time responses was performed.

To model the elastic response of the structures, a multilayer one-dimensional model similar to that of [18] was used. The bond between two contacting layers is considered to be ideal (acoustic mismatch) if displacement of two adjacent points belonging to different materials is the same. However, the case of acoustic mismatch is actually often not realized, especially in case of laminate materials, and such contact is considered to be non-ideal.

To take into account the influence of interface nonideality on the elastic response of the system, a "spring" contact model was used in the calculations. Within this model, the contacting layers are linked to each other with weightless springs evenly distributed over the entire contact area.

In this case the equivalent stiffness of these springs η, which is a quantitative characteristic of the elastic bond of the layers, was one of the key interface parameters in the calculations. The values obtained for the total stiffness of springs and characteristic frequencies of the interfaces under consideration ($f_0 = \eta(Z_1 + Z_2)/2\pi Z_1 Z_2$, where Z_1 and Z_2 are acoustic impedances of contacting layers) are given in Table 1. Frequency f_0 characterizes the frequency dependence of the elastic wave's reflection coefficient at a non-ideal interface [13]:

$$R_{\text{eff}} = \frac{R - if/f_0}{1 - if/f_0},$$

where $R = (Z_1 - Z_2)/(Z_1 + Z_2)$ is the elastic wave's reflection coefficient at a non-ideal interface. For frequencies that are much lower than f_0, $R_{\text{eff}} \approx R$, so the interface can be considered ideal.

For frequencies that are greater than f_0, the value of the elastic wave's reflection coefficient is greater than for the ideal interface case, while the interface is described as non-ideal.

The calculations assumed the fact that the first few tens of picoseconds are not enough for the elastic pulse to propagate throughout the entire heterostructure, so the influence of layers and interfaces manifests itself over time, with different layers and interfaces influencing different parts of the response. This allows to sequentially expand the model by adding new layers to it while increasing the time interval over which the response is analyzed. Layer parameters obtained at the previous stages of calculations are considered to be known. Such technique of fitting-up allows to reduce the modeling time significantly and increase the reliability of parameter determination.

Results

Elastic response was measured in the sample regions having different compositions. Thus, far from the heterostructure, the

response is determined exclusively by the aluminum film and its interface with the Al_2O_3 substrate. As can be seen in Fig. 2*a*, arrival of the laser pulse was immediately followed by a short positive spike of 1–2 ps in duration, which was associated with strong heating of electrons by the pumping radiation, after which damped oscillations were developing smoothly. Two broad peaks can be clearly seen on frequencies of 35 and 120.5 GHz of the Fourier spectrum. These two lines are caused by vibrations of the aluminum film as a whole (low-frequency peak), as well as by with the presence of the elastic pulse repeatedly reflected from the film boundaries (high-frequency peak).

Highlighted in purple in Fig. 2*a* is the modeled response. The calculations allowed estimating the photothermal and photoelastic parameters of the aluminum film, as well as the equivalent stiffness of the interface between the film and the substrate (table). The estimated aluminum thickness (30 nm) perfectly agrees with the value measured with a quartz thickness gauge during the sputtering operation. The spectrum width (Fig. 2*c*) proved to be large for two reasons: due to the leakage of sound wave energy into the sapphire substrate, as well as due to the viscoelastic damping in the polycrystalline Al film (damping length is $1.25\times10^{17}/\omega^2$, m).

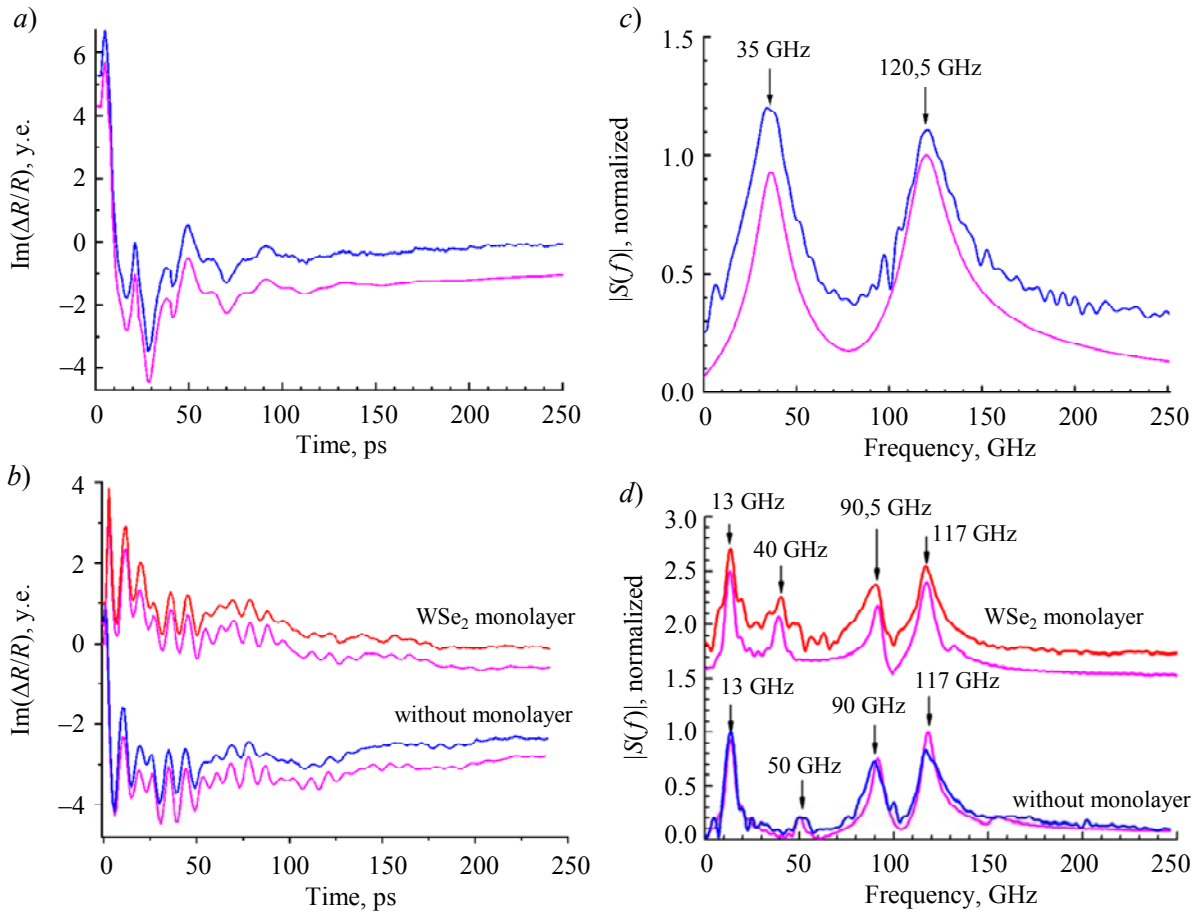

Fig. 2. Experimental dependencies of photoresponse (a and b) and their Fourier spectra (c and d) in the structures: Al/Al_2O_3 – (a and c); Al/hBN/WSe_2(monolayer)/hBN/Al_2O_3 (b and d, red curves) and Al/hBN/hBN/Al_2O_3 (b and d, blue curves). Highlighted in purple in all figures are calculated dependencies

Table

Calculated acoustic parameters of the interfaces under study. AM stands for acoustic mismatch (ideal contact)

Interface	Structure configuration	η, 10^{18} N/мм^3	f_0, GHz
Al/Al_2O_3	Al/Al_2O_3	8.7 ± 2.6	114
Al/hBN	$Al/hBN/hBN/Al_2O_3$	8.4 ± 0.6	258
	$Al/hBN/WSe_2$(monolayer)/hBN/Al_2O_3	2.0 ± 0.7	61.5
hBN/Al_2O_3	$Al/hBN/WSe_2$(monolayer)/hBN/Al_2O_3	AP	
hBN/WSe_2	$Al/hBN/WSe_2$(monolayer)/hBN/Al_2O_3	AP	

The responses from the heterostructure regions without the WSe_2 monolayer ($Al/hBN/hBN/Al_2O_3$, blue curve in Fig. 2*b*) and with the WSe_2 monolayer ($Al/hBN/WSe_2$ (monolayer)/hBN/Al_2O_3, red curve in Fig. 2*b*) have a more complex structure due to the elastic pulse propagation in the hBN layers and WSe_2 monolayer, and the elastic response damps more slowly. Their spectra prove to be more complex because reflections from both Al/hBN, hBN/WSe_2 and hBN/Al_2O_3 interfaces add to natural frequencies. The spectral lines become narrower both due to the increased acoustic length of the system and to the higher reflection coefficient at the hBN/Al_2O_3 interface. Additionally, a characteristic and reproducible feature associated with the presence of the WSe_2 monolayer could be observed in these spectra. It consisted in the shift of the hBN collective mode from 50 GHz to 40 GHz (Fig. 2*d*).

Modeling of experimental responses showed that this feature of the spectra could be described by introducing into the calculation model the δ-distributed mass $m = 1.4\times10^{-5}$ kg/m^2 that corresponds to approximately two masses of the WSe_2 monolayer, which agrees well with photoluminescence measurements and Raman scattering spectroscopy results.

The sensitivity of the collective mode frequency to the WSe_2 monolayer is due to the sufficiently high value of complex reflection coefficient R^* of the δ-distributed mass:

$$R^* = \frac{if / f_0^*}{1 - if / f_0^*},$$

where $f_0^* = \frac{z}{\pi m}$, Z is the wave impedance of the WSe_2 monolayer environment. In this case $f_0^* \sim 160$ GHz, and at $f = 40$ GHz $|R^*| = 0.25$.

Upon estimating the parameter of bond rigidity at the hBN interfaces with a WSe_2 monolayer, these interfaces were found to be described in terms of the ideal contact of layers accurately enough. As for the interface of two hBN layers, the coefficient of reflection from the boundary between them tuned to be equal to zero, that is, the acoustic contact is ideal, and two hBN layers are equivalent to one layer of the total thickness.

The derived feature of the spectrum not only characterizes the WSe_2 monolayer, but also reveals the spectrum sensitivity of the picoacoustic method to the heterostructure composition, and to the individual monolayers as well. To demonstrate this possibility graphically, the responses of the sample region outlined with a white frame in Fig. 3*a* were measured. Then their Fourier spectra were calculated, and the spatial distribution pattern of the modulus of the response spectral component at the frequency of 40 GHz was made, corresponding to the collective mode of the heterostructure with the WSe_2 monolayer (Fig. 3*b*). The structure region comprising the monolayer can be clearly seen in this image. This allowed to locate the WSe_2 monolayer spectrally. Thus,

this research method supplemented by depth profiling of elastic properties which may be used as a tool of hypersonic tomography of such heterostructures.

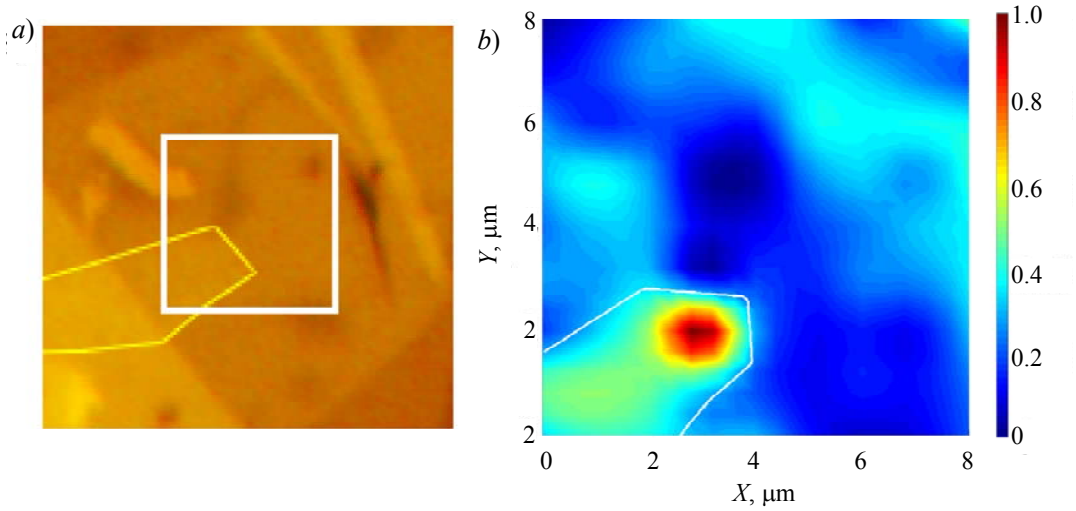

Fig. 3. a) – photo of the structure as seen in the optical microscope, the scanning area is outlined with a white frame; b) – map of the spectral component distribution at the frequency of 40 GHz within the outlined area

Conclusion

Here the elastic properties of the layered heterostructure Al/hBN/WSe_2 (monolayer)/hBN/Al_2O_3 were studied using the optical pump-probe method. The sensitivity of the method proved to be sufficient to spectrally identify the monolayer. This allowed to locate the WSe_2 monolayer acoustically. Modeling of the structure response made enabled estimating the elastic parameters of the WSe_2 monolayer and hBN layers, in particular, determining the rigidity of van der Waals bonds at the structure interfaces.

The results obtained confirm the high potential of the picoacoustic method for characterizing van der Waals materials and heterostructures based on them.

The paper has been prepared with the financial support of the Russian Science Foundation (grant No. 23-22-00444).

REFERENCES

1. Vialla F. and Del Fatti N., Nanomaterials **10** (12), 2543 (2020).
2. Britnell L. et al., Science **335** (6071), 947–950 (2012).
3. Sup Choi M. et al., Nature communications **4** (1), 1624 (2013).
4. Lopez-Sanchez O. et al., Nature nanotechnology **8** (7), 497–501 (2013).
5. Lee H. S. et al., Nano letters **12** (7), 3695–3700 (2012).
6. Gomes L. C. and Carvalho A., Physical Review B **92** (8), 085406 (2015).
7. Chen Y. et al., Advanced Functional Materials **29** (41), 1900959 (2019).
8. Kim J. M. et al., Macromolecular Research **25**, 190–196 (2017).
9. Khan Z. H. et al., Journal of Physics D: Applied Physics **50** (5), 053003 (2017).
10. Fan X. et al., Microsystems & Nanoengineering **6** (1), 17 (2020).
11. Geim A. K. and Grigorieva I. V., Nature **499** (7459), 419–425 (2013).
12. Greener J. D. G. et al., ACS nano **13** (10), 11530–11537 (2019).
13. Greener J. D. G. et al., Physical Review B **98** (7), 075408 (2018).
14. Huang Y. et al., Nature communications **11** (1), 2453 (2020).
15. Pizzocchero F. et al., Nature communications **7** (1), 11894 (2016).
16. Klokov A. Y. et al., Nano Letters **22** (5), 2070–2076 (2022).
17. Tachizaki T. et al., Review of Scientific Instruments **77** (4), 043713 (2006).
18. Klokov A. Y. et al., Journal of Applied Physics **127** (15), (2020).

About authors

Nikolay Yurievich Frolov, junior research assistant, graduate student, Lebedev Physical Institute of the Russian Academy of Sciences (119991, Russia, Moscow, Leninsky Prospect, 53). E-mail: frolil199999@gmail.com SPIN code 1514-3041, Author ID 1288584

Andrey Yuryevich Klokov, leading research assistant, candidate of physics and mathematics, Lebedev Physical Institute of the Russian Academy of Sciences (119991, Russia, Moscow, Leninsky Prospect, 53). E-mail: klokov@lebedev.ru Author ID 121230

Andrey Ivanovich Sharkov, senior research assistant, candidate of physics and mathematics, Lebedev Physical Institute of the Russian Academy of Sciences (119991, Russia, Moscow, Leninsky Prospect, 53). E-mail: shark@sci.lebedev.ru Author ID 33305

Sergey Nikolayevich Nikolaev, senior research assistant, candidate of physics and mathematics, Lebedev Physical Institute of the Russian Academy of Sciences (119991, Russia, Moscow, Leninsky Prospect, 53). E-mail: nikolaev-s@yandex.ru SPIN code 6963-3322, Author ID 880828

Maxim Alexandrovich Chernopitsky, junior research assistant, candidate of physics and mathematics, Lebedev Physical Institute of the Russian Academy of Sciences (119991, Russia, Moscow, Leninsky Prospect, 53). E-mail: 66chemax@gmail.com SPIN code 6529-1510, Author ID 1219510

Semyon Igorevich Chentsov, research assistant, candidate of physics and mathematics, Lebedev Physical Institute of the Russian Academy of Sciences (119991, Russia, Moscow, Leninsky Prospect, 53). E-mail: semtch@gmail.com SPIN code 2361-8799, Author ID 1288583

Mikhail Vladimirovich Pugachev, junior research assistant, Lebedev Physical Institute of the Russian Academy of Sciences (119991, Russia, Moscow, Leninsky Prospect, 53). E-mail: m.pugachev@lebedev.ru

Alexey Vladimirovich Shupletsov, junior research assistant, Lebedev Physical Institute of the Russian Academy of Sciences (119991, Russia, Moscow, Leninsky Prospect, 53). E-mail: shuplecovav@lebedev.ru SPIN code 6413-3082, Author ID 1061429

Vladimir Svyatoslavovich Krivobok, leading research assistant, doctor of physics and mathematics, Lebedev Physical Institute of the Russian Academy of Sciences (119991, Russia, Moscow, Leninsky Prospect, 53). E-mail: krivobokvs@lebedev.ru. Author ID 135304

Alexander Yuryevich Kuntsevich, leading research assistant, doctor of physics and mathematics, Lebedev Physical Institute of the Russian Academy of Sciences (119991, Russia, Moscow, Leninsky Prospect, 53). E-mail: alexkun@lebedev.ru SPIN code 2192-4863, Author ID 160851